$\nabla \cdot \mathbf{B} = 0$ versus the Universe

Ulrich P. Steinwandel^{1★} and Daniel J. Price^{2,3}

¹Max Planck Institute für Astrophysik, Karl-Schwarzschild Str.1, Garching, D-85748, Germany

Accepted XXX. Received YYY; in original form ZZZ

ABSTRACT

We implement the constrained divergence cleaning algorithm of Tricco et al. (2016a) into the cosmological smoothed particle magnetohydrodynamics (SPMHD) code OpenGadget3. Our implementation modifies the governing equations of SPMHD to allow the constrained hyperbolic/parabolic cleaning scheme to be applied consistently in an expanding cosmological framework. This ensures that divergence errors in the magnetic field are actively propagated away and damped, rather than merely being advected with the flow or partially controlled by source terms. To validate our implementation, we perform a series of standard test problems, including the advection of divergence errors, the Orszag-Tang vortex, the Brio-Wu shock tube, and magnetised Zeldovich pancakes. These tests confirm that our scheme successfully reduces divergence errors while preserving the correct physical evolution of the system.

We then apply the method to a fully cosmological simulation of a massive galaxy cluster, comparing the results to those obtained using the previously employed Powell eight-wave divergence preserving scheme, which suppresses divergence growth but does not actively remove it. We find that the overall density structure of the cluster is largely unaffected by the choice of divergence cleaning method, and the magnetic field geometry and strengths in the cluster core remain similar. However, in the cluster outskirts ($r \approx 1-3 \ h^{-1}$ Mpc), the magnetic field is amplified by a factor of 5–10 compared to the Powell-only approach. Moreover, the constrained divergence cleaning algorithm reduces the divergence error by 2–3 orders of magnitude throughout the cluster volume, demonstrating its effectiveness in maintaining the solenoidal condition of the magnetic field in large-scale cosmological simulations. Our results suggest that accurate divergence control is essential for modeling magnetic field amplification in low-density regions of galaxy clusters.

Key words: methods: numerical – magnetohydrodynamics – intracluster medium

1 INTRODUCTION

Our Universe is magnetic. Magnetism extends from the largest structures: galaxies, and the intra-cluster medium (ICM) of galaxy clusters, down to the smallest scales: the interstellar medium (ISM), stars and planets. While magnetic field strengths in stars range from several Gauss (G) in the Sun to 10^{15} G in pulsars, on larger scales B-field strengths typically saturate at the canonical value of a few to a few tens of μ G in galaxies and galaxy clusters but can reach strengths of mG in the dense ISM (Crutcher 2012; Pattle et al. 2023).

Past and current research has developed the following picture of magnetic field amplification in the Universe: A small scale-turbulent dynamo amplifies tiny seed fields to the values we observe today in galaxies and galaxy clusters at μ G-level. The origin of these seed fields is still under debate and several processes have been suggested that can generate seed fields of the order of around 10^{-20} G (e.g. Biermann 1950; Harrison 1970; Demozzi et al. 2009; Gnedin et al. 2000; Durier & Dalla Vecchia 2012). In galaxies, these fields are ordered and influenced by a large-scale (mean-field) α - Ω dynamo (e.g Parker 1955; Steenbeck et al. 1966; Parker 1979; Ruzmaikin

* E-mail: uli@mpa-garching.mpg.de (UPS)

et al. 1988) and can be ejected in galactic outflows that can, in turn, magnetize the circumgalactic medium (CGM) (e.g. Bertone et al. 2006; Pakmor et al. 2017, 2020; van de Voort et al. 2021). However, on galaxy cluster scales in the ICM, turbulence driven by the structure formation processes and merger shocks will quickly generate a saturated magnetic field with a field strength of around $\sim \mu G$ on the scales of Mpc without the need for an explicit seeding of these fields by galactic winds (e.g. Vazza et al. 2018; Steinwandel et al. 2022b). In turn, these fields will be ordered on larger scales by the structure formation process, with some evidence that the Void magnetic field can "remember" the structure of the initial seed field on the scales of a few 10 Mpc (e.g. Mtchedlidze et al. 2022).

The central process behind the turbulent amplification of magnetic fields is the stretch-twist-fold mechanism, introduced by Zel'dovich (1970) and researched by a number of groups (e.g. Kraichnan & Nagarajan 1967; Kazantsev 1968; Kazantsev et al. 1985; Kulsrud & Anderson 1992; Brandenburg et al. 1995; Kulsrud et al. 1997; Xu & Lazarian 2020). On both galaxy and galaxy cluster scales simulations using a variety of methods have established that this process is dominant in amplifying magnetic fields (e.g. Dolag et al. 1999, 2002; Kotarba et al. 2009; Dubois & Teyssier 2008; Wang & Abel 2009; Pakmor & Springel 2013; Pakmor et al. 2017; Butsky et al. 2017;

²School of Physics and Astronomy, Monash University, Clayton, VIC, 3800, Australia

³IPAG, Univ. Grenoble Alpes, CNRS, 38000 Grenoble, France

Garaldi et al. 2021; Steinwandel et al. 2019, 2020, 2022a,b; Vazza et al. 2014, 2018). However, small-scale dynamos can only generate correlated fields on the scale of the turbulence and require a process to order the field on the largest scales. For instance, one can derive the outer scale of MHD turbulence from the peak in the magnetic energy spectra, set by the magnetic Reynolds number which compares the advection timescale to the magnetic diffusion timescale.

Of concern in current MHD simulations of the small scale dynamo in galaxies and galaxy clusters is the degree to which the $\nabla \cdot \mathbf{B} = 0$ condition from Maxwell's equations is enforced. Standard schemes such as constrained transport (Evans & Hawley 1988) cannot be easily ported to Lagrangian particle or moving-mesh schemes employed in cosmological codes, including the Gadget code family (Springel 2005, including GIZMO), and the moving-mesh code AREPO (Springel 2010; though see Mocz et al. 2016). Since the field in cosmological simulations is dynamically weak, errors in the B-field itself are ignorable in that they are unlikely to dramatically change the bulk matter distribution. The approach to date has been to do nothing, a strategy masked by adopting the Powell et al. (1999) 8-wave 'cleaning' scheme. But the 8-wave scheme merely preserves divergence error and does not actively remove it, which can result in errors of order unity in the B-field (e.g. Kotarba et al. 2009; Pakmor & Springel 2013) and possible unphysical B-field amplification (Kotarba et al. 2009).

The hyperbolic/parabolic divergence cleaning scheme proposed by Dedner et al. (2002) is straightforward to adapt to smoothed particle magnetohydrodynamics (SPMHD; Dedner cleaning was first investigated by Price & Monaghan 2005) and moving-mesh codes (Pakmor et al. 2011). However, the scheme was found to be problematic in practice, see e.g. Price (2012) and Pakmor & Springel (2013). Quoting the latter: "a relatively restrictive time-step criterion is required to use the Dedner scheme together with individual time-steps for the cells, and even then it is difficult to guarantee stability in very dynamic environments, encumbering applications to cosmic structure formation". Stasyszyn et al. (2013) implemented Dedner-style cleaning in Gadget, finding that 'in most cases' it improved the results in galaxy cluster simulations. However, their specific choice of numerical operators (which is crucial; see Tricco & Price 2012) was not stated and subsequent attempts to use the vector potential (Stasyszyn & Elstner 2015) suggest that the scheme remained unsatisfactory.

The aspect of being "difficult to guarantee stability" with divergence cleaning was solved by Tricco & Price (2012) by formulating the cleaning equations so as to guarantee energy conservation in the absence of dissipation. Tricco et al. (2016a) extended this stability guarantee to variable cleaning speeds, solving the problem of the "restrictive time-step criterion", since one can set the cleaning speed to the local maximum signal speed for each particle or grid cell, requiring no additional constraint on the timestep. While their scheme was formulated with SPMHD in mind, the principles are general and have been successfully applied in grid-based codes (Derigs et al. 2018; Müller & Varma 2020; Varma & Müller 2021).

One of us (DJP) subsequently enjoyed the last decade applying SPMHD with constrained hyperbolic/parabolic cleaning to magnetised star formation, enabling stable calculations of magnetised jets (Price et al. 2012; Bate et al. 2014; Wurster et al. 2018) which would previously explode (Tricco & Price 2012), non-ideal MHD (e.g. Wurster et al. 2014, 2016, 2017, 2018, 2019), magnetic fields in isolated galaxies (Dobbs et al. 2016) and — most relevant to this paper — a code comparison on the small scale dynamo (Tricco et al. 2016b). However, while default in the Phantom SPMHD code used in star and planet formation (Price et al. 2018), the constrained cleaning algorithm has never been fully implemented in the Gadget

family of cosmological SPMHD codes and hence not applied to simulations on the largest scales of the Universe. By good fortune, the other of us (UPS) is an expert in galaxy clusters. Our paths collided.

The main result of our collaboration, presented in this paper, is a simulation of a massive galaxy cluster with a total mass of $2\times 10^{15}~M_{\odot}$ modeled with and without active cleaning of divergence errors in the magnetic field. We study the amplification of the field at a resolution that is high enough to resolve the Coulomb collision scale in the ICM and assess the effect of magnetic fields on the thermal pressure profile of the cluster. Our main aim is to test the importance of active control of divergence errors in such simulations.

The paper is structured as follows: In Section 2, we discuss our implementation of the constrained cleaning scheme in OpenGadget3. Appendix A gives the results of test problems to ensure our scheme is working. Our main results (Section 3) are cosmological simulations of a massive galaxy cluster with and without the newly implemented cleaning scheme. We discuss in Section 4 and conclude in Section 5.

2 METHODS

2.1 Simulation Code

The end goal of this paper is to implement the constrained divergence cleaning scheme of Tricco & Price (2012) and Tricco et al. (2016a) into the cosmological simulation code OpenGadget-3 (CITE). The code is the developer base of the code P-Gagdet-2/3 (Springel 2005) and is a Tree-multi-method code that can treat hydrodynamics via SPH in density-entropy and pressure-entropy formulation as well as via the meshless finite mass (MFM) method (Groth et al. 2023). Furthermore, the code has the ability to solve for the MHD equations in SPMHD in density-entropy formulation. Hence, the code needs to solve the equations of ideal MHD

$$\frac{\mathrm{d}\rho}{\mathrm{d}t} = -\rho(\nabla \cdot \mathbf{v}) \tag{1}$$

$$\frac{\mathrm{d}\mathbf{v}}{\mathrm{d}t} = -\frac{\nabla P}{\rho} + \mathbf{g} + \frac{(\mathbf{J} \times \mathbf{B})}{\rho},\tag{2}$$

$$\frac{\mathrm{d}\mathbf{B}}{\mathrm{d}t} = (\mathbf{B} \cdot \nabla)\mathbf{v} - \mathbf{B}(\nabla \cdot \mathbf{v}),\tag{3}$$

$$\frac{\mathrm{d}K}{\mathrm{d}t} = \frac{\gamma - 1}{\rho^{\gamma - 1}} \Lambda_{\mathrm{diss}} \tag{4}$$

$$\nabla \cdot \mathbf{B} = 0, \tag{5}$$

where $d/dt \equiv \partial/\partial t + \mathbf{v} \cdot \nabla$ is the Lagrangian time derivative, ρ is the density, \mathbf{v} is the velocity, P is the pressure, \mathbf{J} is the current, \mathbf{B} is the magnetic field, $K \equiv P/\rho^{\gamma}$ is the entropy variable and $\Lambda_{\rm diss}$ represents any energy dissipated at shocks or current sheets.

Without going to much into detail about the underlying SPMHD framework we want to point out how the formulation of Eq. 3 is important. For that we consider the induction equation written in Eulerian form

$$\frac{\partial \mathbf{B}}{\partial t} = \nabla \times (\mathbf{v} \times \mathbf{B}) \tag{6}$$

$$= -(\mathbf{v} \cdot \nabla)\mathbf{B} + (\mathbf{B} \cdot \nabla)\mathbf{v} - \mathbf{B}(\nabla \cdot \mathbf{v}) + \mathbf{v}(\nabla \cdot \mathbf{B}), \tag{7}$$

which can be written as Eq. 3 only if the last term is neglected.

2.2 Divergence preservation and the Powell scheme in Gadget

The advantage of solving Eq. 3 instead of Eq. 6 becomes clear when we take the divergence of Eq. 3, which yields:

$$\frac{\partial}{\partial t} (\nabla \cdot \mathbf{B}) + \nabla \cdot (\mathbf{v} \nabla \cdot \mathbf{B}) = 0.$$
 (8)

This equation has a similar form to the continuity equation (Eq. 1; in Eulerian form reading $\partial \rho / \partial t + \nabla \cdot (\mathbf{v}\rho) = 0$). By analogy with conservation of mass ($\int \rho dV$), this implies that

$$\int (\nabla \cdot \mathbf{B}) dV = \oint_{S} \mathbf{B} \cdot d\mathbf{S} = \text{const}, \tag{9}$$

and hence that the global magnetic surface flux is conserved, even in the presence of $\nabla \cdot \mathbf{B}$ errors in the simulation domain. Hence, this form of the induction equation is monopole conserving — but not destroying — by construction. Furthermore, every SPMHD implementation needs to address the issue of an (unphysical) source term in the momentum equation that scales as $\nabla \cdot \mathbf{B}$ (see discussion in Price 2012). This term typically arises because the force related to MHD is written as a divergence of the MHD stress tensor. This term gives rise to the tensile instability where this term leads to an attractive force that dominates when the magnetic pressure exceeds the gas pressure (Phillips & Monaghan 1985; Morris 1996; Price 2012). In GADGET, as in other SPMHD codes (including PHANTOM; Price et al. 2018), this source term is subtracted from the momentum equation following Børve et al. (2001), which yields an overall scheme equivalent to the Powell et al. (1999) "8 wave scheme" in SPH formulation. Hence, every stable numerical SPMHD scheme enforces a monopole-preservation scheme similar to the Powell et al. (1999) approach by construction.

2.3 New Constrained Divergence-Cleaning in Gadget

We follow the constrained cleaning approach derived by Tricco et al. (2016a) to improve GADGET's default divergence-preservation scheme above. We will briefly go over the derivation of the constrained cleaning equations of Tricco et al. (2016a) with the difference that we will apply the appropriate correction terms that arise from GADGET's unit system in comoving units when cosmological simulations are carried out.

The scheme of Tricco et al. (2016a) is itself a formulation of the scheme of Tricco & Price (2012) adapted for a variable cleaning speed and is based on the original scheme of Dedner et al. (2002). The underlying idea is that the induction equation is corrected by the gradient of a scalar field ψ yielding the following equations

$$\frac{\mathrm{d}\mathbf{B}}{\mathrm{d}t} = (\mathbf{B} \cdot \nabla)\mathbf{v} - \mathbf{B}(\mathbf{v} \cdot \nabla) - \nabla\psi,\tag{10}$$

$$\frac{\partial \psi}{\partial t} = -c_h^2 (\nabla \cdot \mathbf{B}) - \frac{\psi}{\tau}. \tag{11}$$

One can combine them to obtain a damped wave equation for the magnetic field divergence error leading to

$$\frac{\partial^{2}(\nabla \cdot \mathbf{B})}{\partial t^{2}} - c_{h}^{2} \nabla^{2}(\nabla \cdot \mathbf{B}) + \frac{1}{\tau} \frac{\partial(\nabla \cdot \mathbf{B})}{\partial t} = 0, \tag{12}$$

where τ is given via:

$$\tau = \frac{h}{\sigma c_{\rm h}},\tag{13}$$

with the cleaning speed c_h , and a dimensionless numerical constant 1

 σ (typically $\sigma=1$ in three dimensional simulations; see Tricco & Price 2012). From Eq. 12 it becomes clear that this scheme spreads the divergence over a larger (non-local) domain and damps it as function of time. Tricco & Price (2012) showed that the classic Dedner et al. (2002) approach is unstable at density jumps which can lead to an exponential and unbounded growth in magnetic energy, which is Not A Good ThingTM. Tricco & Price (2012) showed that the scheme can be stabilized against this instability by making sure that energy conservation is established between the energy that is stored in the magnetic fields as well as the energy that is deposited in the cleaning field ψ . This ensures that the inclusion of the parabolic terms monotonically decreases the magnetic energy. The cleaning equations of Tricco & Price (2012) read

$$\frac{\mathrm{d}\mathbf{B}}{\mathrm{d}t} = (\mathbf{B} \cdot \nabla)\mathbf{v} - \mathbf{B}(\nabla \cdot \mathbf{v}) - \nabla\psi, \tag{14}$$

$$\frac{\mathrm{d}\psi}{\mathrm{d}t} = -c_{\mathrm{h}}^{2}(\nabla \cdot \mathbf{B}) - \frac{\psi}{\tau} - \frac{1}{2}\psi(\nabla \cdot \mathbf{v}). \tag{15}$$

These equations revert back to a Powell et al. (1999) scheme for vanishing ψ . However, these equations are strictly only valid as long as c_h and τ are spatially and temporally constant. Hence, Tricco et al. (2016a) derived a version which allows for a variable cleaning speed c_h that can be derived from energy arguments and the discussion of additional source terms when the cleaning speed c_h is non-constant. Specifically, one will see (Tricco et al. 2016a) that for non-constant cleaning speed there is a source term of the form dc_h/dt . The trick is now to handle that term simultaneously with $d\psi/dt$. Thus instead of evolving $d\psi/dt$, we evolve $d(\psi/c_h)/dt$. This leads to a system of equations that reads

$$\frac{1}{a^2} \frac{d\mathbf{B}}{dt} = (\mathbf{B} \cdot \nabla)\mathbf{v} - \mathbf{B}(\nabla \cdot \mathbf{v}) - \nabla \psi, \tag{16}$$

$$\frac{1}{a^2} \frac{\mathrm{d}}{\mathrm{d}t} \left(\frac{\psi}{c_{\mathrm{h}}} \right) = -c_{\mathrm{h}} (\nabla \cdot \mathbf{B}) - \frac{1}{\tau} \left(\frac{\psi}{c_{\mathrm{h}}} \right) - \frac{1}{2} \left(\frac{\psi}{c_{\mathrm{h}}} \right) (\nabla \cdot \mathbf{v}), \tag{17}$$

which can be discretized in SPH in comoving units for cosmological integration according to

$$\frac{1}{a^2} \left(\frac{\mathrm{d} \mathbf{B}_i}{\mathrm{d} t} \right)_{\psi} = -\rho_i \sum_j m_j \left[\frac{\psi_i}{\Omega_i \rho_i^2} \nabla_i W_{ij}(h_i) + \frac{\psi_j}{\Omega_j \rho_j^2} \nabla_i W_{ij}(h_j) \right],\tag{18}$$

$$\frac{1}{a^2} \frac{\mathrm{d}}{\mathrm{d}t} \left(\frac{\psi}{c_{\mathrm{h}}} \right)_i = \frac{c_{\mathrm{h},i}}{\Omega_i \rho_i} \sum_j m_j (\mathbf{B}_i - \mathbf{B}_j) \cdot \nabla_i W_{ij}(h_i) - \frac{1}{\tau} \left(\frac{\psi}{c_{\mathrm{h}}} \right)_i \tag{19}$$

$$+\frac{1}{2}\left(\frac{\psi}{c_{\rm h}}\right)_{i}\sum_{i}m_{j}(\mathbf{v}_{i}-\mathbf{v}_{j})\cdot\nabla_{i}W_{ij}(h_{i}),\tag{20}$$

where W is the kernel, i and j the indices of the particles over which we carry out the SPH sum and h is the smoothing length. The only difference between the version of these equations written down in Tricco et al. (2016a) and our work is the inclusion of the appropriate units for comoving integration which is denoted as the scale factor a in the equations above. We adopt

$$c_{\rm h} = \sqrt{v_A^2 + c_s^2},\tag{21}$$

with the Alfven-speed v_A^2 and the sound-speed c_s . This choice can be tied to an "Overcleaning factor" ζ by a timestep constraint based on

$$\Delta t = \min\left(\frac{C_{\text{courant}}h}{V_{\text{sig}}}, \frac{C_{\text{courant}}}{\zeta c_{\text{h}}}\right),\tag{22}$$

cleaningParabolicSigma" and has a default value when the code is run in three dimensions that defaults to one.

¹ This is implemented in our code as a parameter file option called "DivB-

4 UPS and DJP

noting that with $\zeta = 1$ that the timestep is not changed at all by the cleaning condition, since in general $c_h < v_{\text{sig}}$ if Eq. 21 is used. Typically $C_{\text{courant}} = 0.3$ (e.g. Monaghan & Lattanzio 1985).

2.4 Simulations and Initial Conditions

In this work we aim to present the initial implementation and testing of the constrained cleaning scheme of Tricco & Price (2012) and Tricco et al. (2016a), adapted for the use in cosmological simulations. The results of our implementation tests are given in Appendix A. We focus on the application of the scheme to massive galaxy clusters, using the 'nifty cluster' as our test-bed for quantifying the scheme in a cosmological context. The initial conditions (ICs) for the cluster are taken from the MUSIC-2 sample (e.g. Prada et al. 2012; Sembolini et al. 2013, 2014; Biffi et al. 2014) that has been later utilized for a cluster comparison project in the nifty collaboration (hence the nifty cluster; Sembolini et al. 2016). The cluster has the following physical properties: The clusters mass $M_{200c} = 10^{15} M_{\odot}$ and is selected as zoom-in initial condition from a large Gpc-volume. The dark matter mass resolution is $m_{dm} = 9.01 \times 10^8~h^{-1}~M_{\odot}$ and a gas resolution of $m_{gas} = 1.9 \times 10^8 \text{ h}^{-1} \text{ M}_{\odot}$. This makes the resolution similar to early simulations of galaxy cluster formation with the focus on magnetic field amplification (e.g. Dolag et al. 1999, 2001, 2002, 2004, 2005; Dolag & Stasyszyn 2009; Bonafede et al. 2011; Vazza et al. 2011; Stasyszyn et al. 2010, 2013) or the lowest resolution runs in Steinwandel et al. (2022b), Vazza et al. (2014) and Vazza et al. (2018). This mass resolution is ideal for testing and development as we can complete on run down to redshift zero in approximately a few hours. Ten or a hundred times higher resolution are drastically more expensive (weeks to months) (see e.g., Steinwandel et al. 2022b, 2023, for simulations with much higher resolution). The background cosmology of the box follows a WMAP7 cosmology (Komatsu et al. **2011**) with $\Omega_{\rm m} = 0.27$, $\Omega_{\rm b} = 0.0469$, $\Omega_{\Lambda} = 0.73$, $\sigma_8 = 0.82$, n = 0.95 and h = 0.7. We use Subfind to identify haloes (Springel et al. 2001; Dolag et al. 2009). For these run we further adopt physical (isotropic) conduction with a Spitzer suppression value of 0.05. We performed five simulations of this cluster with i) No cleaning (niftynoclean); ii) constrained cleaning in the default setting (nifty-clean); iii) constrained cleaning with a timestep criterion that allows for faster cleaning than the cleaning speed defined via Eq. 21 (nifty-clean2) iv) a simulation in which we test the contribution of the advection term in Eq. 17 (nifty-advect) and v) the contribution of converting the energy stored in the cleaning equations back to thermal energy (nifty-heat).

3 RESULTS

Fig. 1 shows column-density projections (top row; $\int \rho dz$) and column-averaged internal energy ($\langle u \rangle \equiv \int \rho u dz / \int \rho dz$; bottom row), for the models nifty-noclean, nifty-clean and nifty-clean 2 (left to right).

We find only minor differences in the global evolution of these quantities due to the inclusion of the new cleaning scheme. However, the central density in the run nifty-noclean is slightly higher by roughly a factor of two than in the runs nifty-clean and nifty-clean2, the origin of which we will discuss in greater detail in Sec. 4. For now it is sufficient to note that this effect is related to whether or not we dissipate the energy stored in the cleaning field as heat.

Fig. 2 shows a slice of the magnetic field strength (top row) and the column-averaged relative divergence of the field (bottom row), again for the three runs nifty-noclean, nifty-clean and nifty-clean2

(left to right). The magnetic field in the runs with the new constrained cleaning of Tricco et al. (2016a) is more spread out. Again, some of this originates from how we chose to dissipate the energy stored in the cleaning field — we discuss the details in Section 4. The bottom row reveals that the new scheme outperforms GADGET's older Powell divergence-preservation scheme by at least 2.5 orders of magnitude. The effect of cleaning with twice the signal speed as presented in the left column of Fig. 2 shows only very marginal improvement over the default scheme where the cleaning speed is given via Eq. 21. All three simulations have a similar run time down to the 2 per cent level. That is, the new improved cleaning comes essentially for free. However, we note that if we clean faster than a factor of four than the cleaning speed defined by Eq. 21 the code starts to slow down dramatically.

In Fig. 3 we show the mean magnetic field strength within the virial radius of the simulated cluster as a function of scale factor (left panel) and the evolution of the relative divergence as function of scale factor (right panel). Interestingly, we find that with divergence cleaning the field grows at a slightly steeper rate than without the divergence cleaning prescription. We attribute this to excess dissipation of magnetic energy in simulations with high divergence errors due to unphysical small-scale noise in the magnetic field, an effect also seen in turbulence simulations in SPH where insufficient shock viscosity can lead to excess dissipation of energy (Price & Federrath 2010). Tricco & Price (2012) also showed that divergence cleaning could produce much better control of divergence errors without excessively dissipating magnetic energy, compared to using artificial resistivity alone. Hence divergence cleaning leads to an effectively higher magnetic Prandtl number.

It is clear from the right hand panel of Fig. 3 that the mean divergence error as function of scale factor is reduced by at least one order of magnitude. We also measure the relative divergence error in the regions that exceed the initial seed field to quantify the divergence in the regions where the magnetic field is strongly amplified, which we plot as the dashed lines for each run. It is interesting to note that the divergence is generally speaking lower in the regime where the magnetic field is strong, even in the case where there is only the Powell cleaning scheme applied where we find that the divergence is lower in the highly magnetized regions at the end of the simulations by roughly a factor of four. While this trend is somewhat present in the two runs nifty-clean and nifty-clean2 it is weaker and the divergence in the magnetized regions is only factor of two lower than in the whole simulation region. The advection term in the cleaning equations as well as the exact way we choose to dissipate the energy stored in the cleaning equations does not have a strong effect on the outcome of any of these quantities, manifesting in the fact that the runs nifty-advect and nifty-heat do not change the relative divergence very strongly. However, they do affect the saturation value of the field down to redshift zero, where the run nifty-heat where we do not convert the energy stored in the cleaning field to heat. This leads to higher central densities and thus lower entropy in the core. Hence, the magnetic field is adiabatically compressed in this run and the saturation value is increasing.

In Fig. 4 we show the radial profiles of the magnetic field strength on the left as well as the radial profiles of the relative divergence of the magnetic field. As expected from investigation of the first row of Fig. 2 we find that in the simulations with the new active cleaning scheme following the prescription of Tricco et al. (2016a), the magnetic field strength out larger radii is higher by roughly half a dex compared to the run with active Powell-cleaning nifty-noclean. It is interesting to note that the magnetic field strength in the run nifty-heat drops quicker than in the other runs with the new cleaning

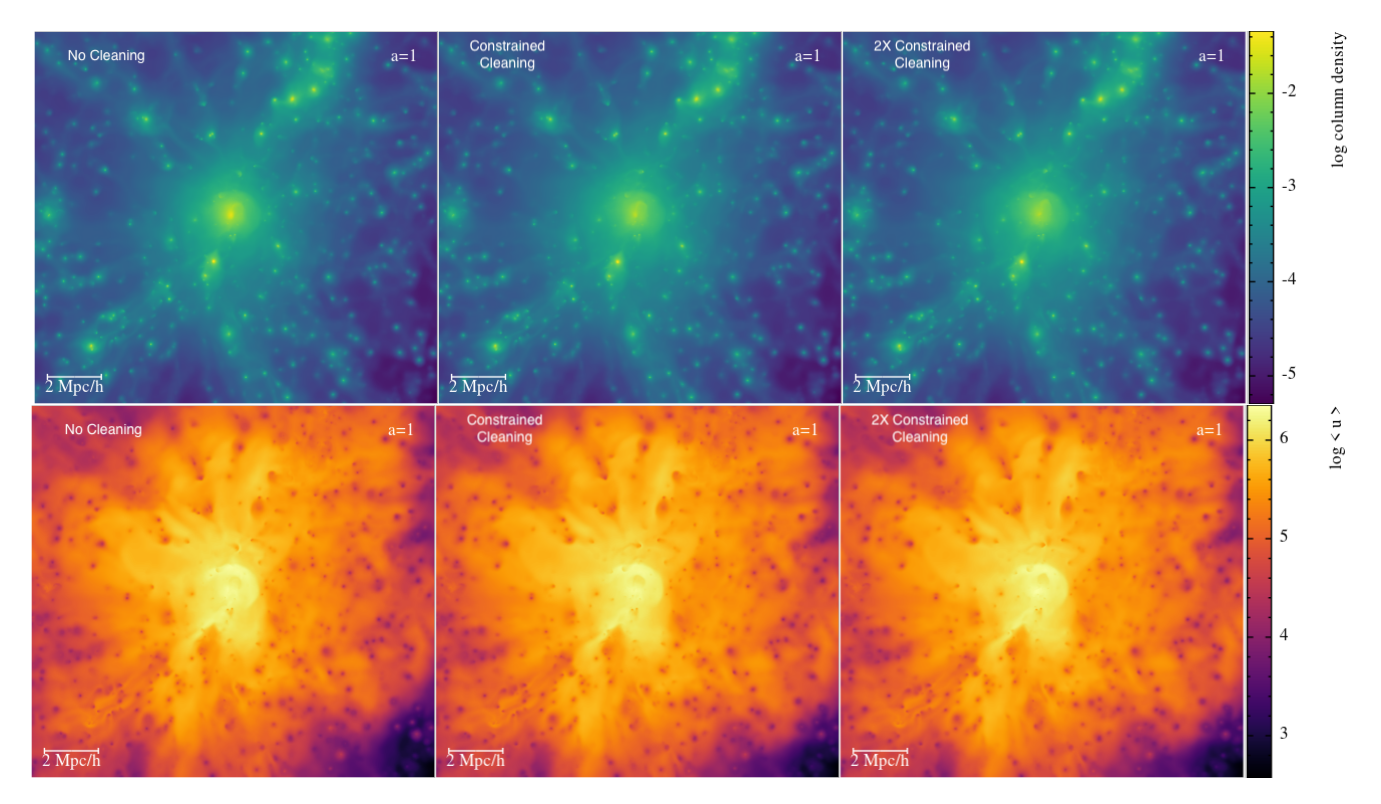


Figure 1. Top row: Column density projections for our cluster for three of our runs, nifty-noclean (left), nifty-clean (centre) and nifty-clean2 (right). The central density in the run nifty-noclean is higher than in the runs nifty-clean and nifty-clean2. Bottom row: Internal energy of the different clusters, the thermal structure is remains very similar in the three runs.

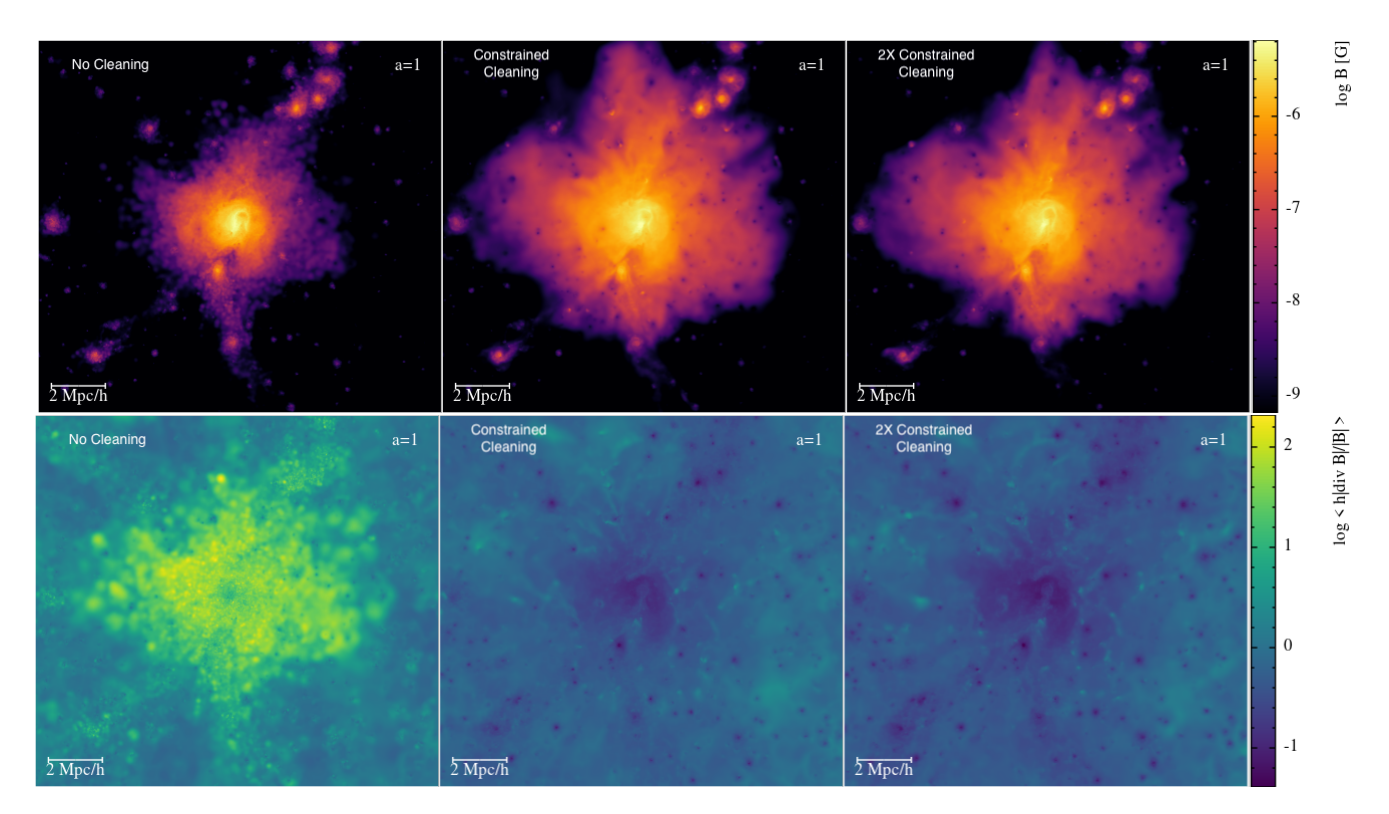
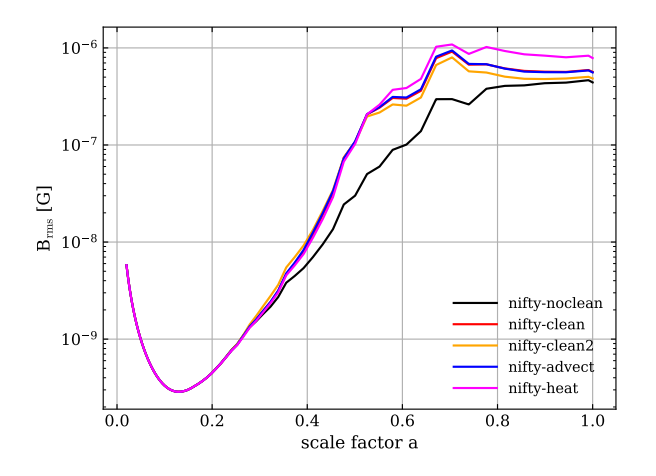


Figure 2. *Top row:* Magnetic field strength for the simulations nifty-noclean (left), nifty-clean (centre) and nifty-clean2 (right). The magnetic field strength in the runs with active cleaning is more spread out than in the run without cleaning. We will discuss the reason for this in more detail in Sec. 4. *Bottom row:* Normalized divergence within the cluster for the three models. We finds divergence errors reduced by up to three orders of magnitude in the central regions of the cluster in the nifty-clean and nifty-clean2 calculations.



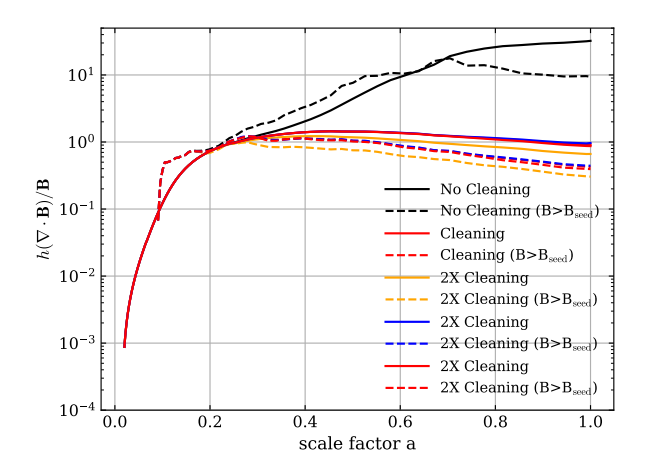
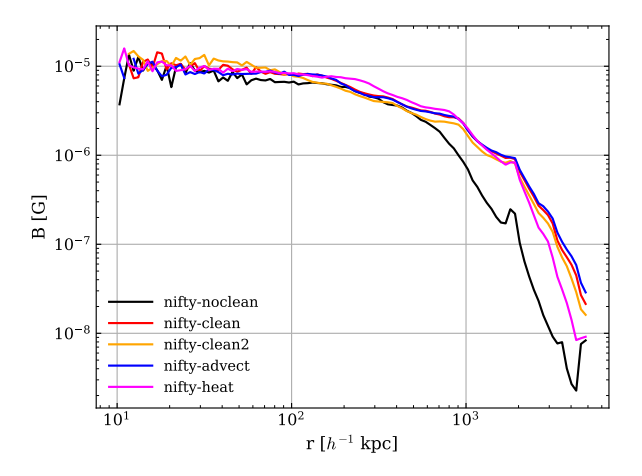


Figure 3. Mean divergence error as a function of scale factor for the magnetized nifty cluster. The solid lines represent the mean over the whole volume, while the dashed lines show the field mean over the particles that possess a field that is higher than the initial (physical) seed field of 10^{-8} G. The black lines show the results without cleaning, the red lines with the new fiducial cleaning approach, and the golden lines a cleaning approach that adopts faster cleaning than the fastest wave speed by a factor of two.



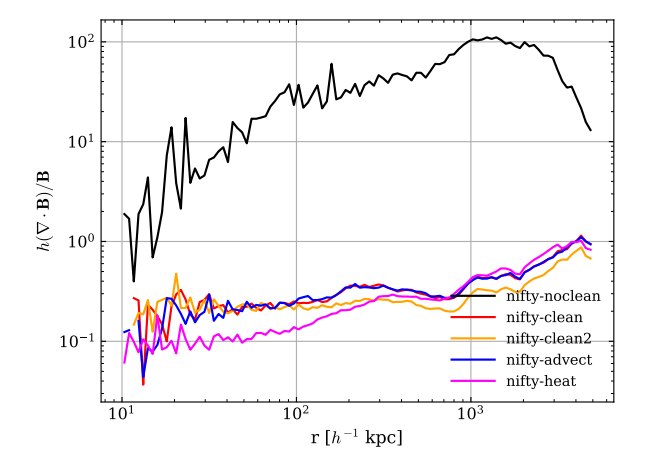


Figure 4. Radial profiles of the magnetic field (left), the relative divergence error (center) and the entropy (left) for the magnetized version of the nifty cluster in runs without cleaning (black), the new fiducial constrained cleaning scheme (red) as well as in a simulation with 2× faster cleaning than the fastest wave speed.

scheme. This implies that some of this behavior can be explained by an increase of diffusivity when we include the conversion of the energy stored in the cleaning field ψ to heat. However, the magnetic field strength in radial profile is still higher in all the run in which we include the new constrained cleaning prescription. The radial profile of the relative divergence reveals that the divergence error is at least one order of magnitude lower in all runs compared to the run nifty-noclean.

Fig. 5 shows the radial entropy profiles for all five runs that we carried out. The entropy profiles of the cluster turns out to be most sensitive to the the numerical details of the cleaning scheme that is adopted. For instance, the run nifty-heat has the lowest entropy in the cluster centre. This is consistent with the highest magnetic fields at saturation in this run in the time-evolution in the left hand panel of Fig. 3. The reason that the entropy is the lowest in nifty-heat is relate to the fact that this run does not have an additional source term for the entropy while in all the other runs we dissipate the energy

stored in the cleaning field as heat back into the systems. Hence, this is literally a source of entropy where the cleaning speed is high, i.e. in the center of the cluster. The reason that the entropy is larger in the run nifty-clean2 in the central regions is related of the fact that the cleaning is faster by a factor of two, dissipating the energy more effectively. The outskirts of the cluster show convergence in the entropy profile, independent of the details of the adopted cleaning scheme. We note that there is no consensus to this day on what the exact shape of the cluster entropy profile should be, but it is apparent that the cleaning scheme can affect this, specifically if we choose to add the energy stored in the cleaning field ψ as an additional source term for the entropy. Historically, SPH struggles with cored entropy profiles in non-radiative simulations of galaxy cluster formation and thus it is interesting to point out that with active cleaning we find a tendency to realize a cored cluster profile.

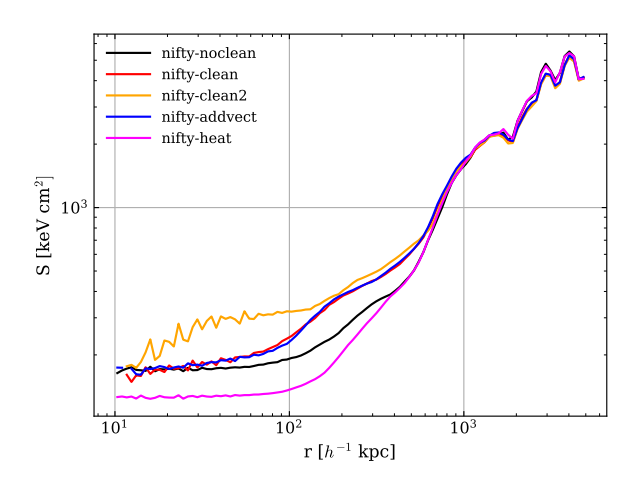


Figure 5. Radial entropy profiles of our simulated clusters. The entropy profile is quite sensitive to the adopted cleaning method, which is important to point out. The entropy core in the cluster can actually be stabilized with higher cleaning speed, when we convert the energy stored in the cleaning field into heat, i.e. following eq. 21 of Tricco et al. (2016a). If we exclude this term the entropy core settles at a lower value. Removing the advection term from the cleaning scheme has a rather little impact on the entropy profile.

4 DISCUSSION

The clusters morphology remains mostly unchanged by the inclusion of the constrained divergence cleaning scheme of Tricco et al. (2016a), although we note that the there is some change in the central density of the cluster. We find that the central density of the cluster is lower in the runs nifty-clean and nifty-clean2, when directly compared to the run nifty-noclean. It is a priori not quite clear why this occurs, hence we tested a few variations in the runs where we switched off the conversion of the energy stored in the cleaning field ψ to thermal energy (nifty-heat), as well as the contribution to the cleaning to the advection term in Eq. 20 (nifty-advect). It turns out that the advection term appears to be rather unimportant for the solution and only plays a minor role when it comes to the time and radial evolution of the quantities that we plot in Fig. 3, Fig. 4 and Fig. 5. This is very similar as reported by Tricco & Price (2012) and Tricco et al. (2016a). This is an important remark since it is not clear that in a galaxy cluster with a virial velocity of $\sim 1000 \text{ km s}^{-1}$ with strong accretion in the central dark matter potential the velocity divergence is small. However, our tests suggested that the advection term is subdominant in comparison to the hyperbolic and parabolic cleaning terms. There is a larger impact on the time evolution of the magnetic field and the radial profiles of magnetic field, relative divergence and entropy, related to the choice on how to treat the energy stored in the cleaning field ψ . If we choose to dissipate the energy into thermal energy and by adding a source term for the entropy, we find that the magnetic field strength increases, while the divergence towards the cluster center is decreasing by roughly a factor of two. The most interesting change related to this choice is affecting the entropy profile, where we find that the run nifty-heat has the lowest entropy in the cluster center. This makes sense, as we removed the additional source term for entropy that is coupled back to the system. The run nifty-noclean has the second lowest central entropy, while the cleaning runs nifty-clean and nifty-clean2 have the highest central entropy. The run nifty-advect is almost identical to the run nifty-clean, again confirming that the advection term is of minor importance to the

systems evolution (at least with respect to the entropy profile). The run nifty-clean2 has the highest central entropy which as this run has a factor of two increased cleaning speed and hence a factor of four faster conversion of "cleaning energy" to thermal energy than the run nifty-clean, which shows clearly up in the entropy profile. Hence, the choice we made to actively dissipate the energy stored in the ψ is actually affecting the cluster center. It is debatable if that is good or bad. However, we note that the effect is similar to what is expected from galaxy cluster simulations with physical conduction and high values (30 to 100 per cent) for the Spitzer suppression factor of the thermal conductivity. We find a significant change in the magnetic field structure in the runs nifty-clean and nifty-clean2 compared to the run nifty-noclean, where we see that the magnetic field is extending to higher values, further out in the halo. At first, this might be counter-intuitive as one would expect that when the divergence of the field is reduced the magnetic field strength should follow that trend. However, this is not necessarily true, since the divergence operator has a sign. Its also important to note that this effect is mostly restricted to the region beyond the virial radius of the system at around ~ 1.5 Mpc, where the resolution becomes really poor. We note that part of the effect can again be attributed due the dissipation of energy in the cleaning field ψ as the run nifty-heat has the lowest field strength in the cluster outskirts. This is again consistent with observations made in higher resolution simulations of galaxy clusters and varying Spitzer-suppression factors for the thermal conductivity.

5 CONCLUSIONS

We have demonstrated the following key results:

- (i) Implementing the Tricco et al. (2016a) constrained divergence cleaning algorithm in OpenGadget3 leads to a dramatic reduction in divergence errors in cosmological simulations of galaxy clusters. Specifically, divergence errors are reduced by 2–3 orders of magnitude relative to the previously employed Powell-only SPMHD scheme in Gadget, which merely preserves the divergence without actively removing it. This improvement ensures that the magnetic field remains closer to the physically required solenoidal condition, enhancing the overall reliability of the simulation results.
- (ii) Large divergence errors, as observed in simulations that rely solely on the Powell scheme, have a systematic impact on the properties of the magnetic field, particularly in the outer, poorly resolved regions of clusters. In these regions, the growth of magnetic energy through dynamo amplification is suppressed, and the magnetic field strengths are generally underestimated. By actively controlling divergence, the constrained cleaning scheme allows for more accurate representation of field amplification processes, capturing stronger magnetic fields and more realistic dynamo behavior in low-density, under-resolved cluster outskirts.
- (iii) The cleaning scheme also improves the qualitative appearance of the magnetic field. Compared to simulations without cleaning, the resulting field is overall smoother and less patchy, with coherent structures extending over larger regions. This smoother field distribution not only better reflects the expected physical behavior of magnetised plasma in galaxy clusters but also helps reduce numerical artifacts that can arise from irregular, spurious divergence in under-resolved regions.
- (iv) Even in simulations with comparatively low resolution, the inclusion of divergence cleaning leads to magnetic field geometries that are in closer agreement with those obtained in higher-resolution simulations. This consistency indicates that the cleaning scheme not only reduces numerical errors but also stabilizes the evolution of the

magnetic field across different resolutions, improving the physical fidelity and robustness of the results. As a result, conclusions drawn about the magnetic structure of galaxy clusters become more reliable, even when computational limitations prevent extremely high resolution

Furthermore, the new energy-conserving cleaning scheme introduces no additional computational overhead and is now publicly available within the OpenGadget3 code, providing the community with a practical and efficient tool for conducting accurate magnetohydrodynamical simulations in a cosmological context.

ACKNOWLEDGEMENTS

UPS and DJP thank the organizers of the Flatiron Center for Computational Astrophysics 2023 fluid dynamics summer school for inviting them both to teach, during which this project was initiated. The simulation code and the simulations in this work have been carried out on the Flatiron in-house cluster "rusty". UPS thanks Ludwig Böss, Klaus Dolag, Rüdiger Pakmor and Volker Springel for insightful comments. DJP thanks N. Cuello, F. Ménard and everyone in Grenoble for hosting him on sabbatical where this paper was completed.

DATA AVAILABILITY

The data in this paper will be made available based on reasonable request to the corresponding author.

REFERENCES

```
Bate M. R., Tricco T. S., Price D. J., 2014, MNRAS, 437, 77
Bertone S., Vogt C., Enßlin T., 2006, MNRAS, 370, 319
Biermann L., 1950, Zeitschrift Naturforschung Teil A, 5, 65
Biffi V., Sembolini F., De Petris M., Valdarnini R., Yepes G., Gottlöber S.,
    2014, MNRAS, 439, 588
Bonafede A., Dolag K., Stasyszyn F., Murante G., Borgani S., 2011, MNRAS,
    418, 2234
Børve S., Omang M., Trulsen J., 2001, ApJ, 561, 82
Brandenburg A., Moss D., Shukurov A., 1995, MNRAS, 276, 651
```

Crutcher R. M., 2012, ARA&A, 50, 29 Dedner A., Kemm F., Kröner D., Munz C. D., Schnitzer T., Wesenberg M.,

Brio M., Wu C. C., 1988, Journal of Computational Physics, 75, 400

Butsky I., Zrake J., Kim J.-h., Yang H.-I., Abel T., 2017, ApJ, 843, 113

2002, Journal of Computational Physics, 175, 645

Dehnen W., Aly H., 2012, MNRAS, 425, 1068

Demozzi V., Mukhanov V., Rubinstein H., 2009, J. Cosmology Astropart. Phys., 2009, 025

Derigs D., Winters A. R., Gassner G. J., Walch S., Bohm M., 2018, Journal of Computational Physics, 364, 420

Dobbs C. L., Price D. J., Pettitt A. R., Bate M. R., Tricco T. S., 2016, MNRAS, 461, 4482

Dolag K., Stasyszyn F., 2009, MNRAS, 398, 1678

Dolag K., Bartelmann M., Lesch H., 1999, A&A, 348, 351

Dolag K., Schindler S., Govoni F., Feretti L., 2001, A&A, 378, 777

Dolag K., Bartelmann M., Lesch H., 2002, A&A, 387, 383

Dolag K., Jubelgas M., Springel V., Borgani S., Rasia E., 2004, ApJ, 606,

Dolag K., Vazza F., Brunetti G., Tormen G., 2005, MNRAS, 364, 753

Dolag K., Borgani S., Murante G., Springel V., 2009, MNRAS, 399, 497

Dubois Y., Teyssier R., 2008, A&A, 482, L13

Durier F., Dalla Vecchia C., 2012, MNRAS, 419, 465

Evans C. R., Hawley J. F., 1988, ApJ, 332, 659

Garaldi E., Pakmor R., Springel V., 2021, MNRAS, 502, 5726

```
Gnedin N. Y., Ferrara A., Zweibel E. G., 2000, ApJ, 539, 505
```

Groth F., Steinwandel U. P., Valentini M., Dolag K., 2023, MNRAS, 526, 616 Harrison E. R., 1970, MNRAS, 147, 279

Kazantsev A. P., 1968, Soviet Journal of Experimental and Theoretical Physics, 26, 1031

Kazantsev A. P., Ruzmaikin A. A., Sokolov D. D., 1985, Zhurnal Eksperimentalnoi i Teoreticheskoi Fiziki, 88, 487

Komatsu E., et al., 2011, ApJS, 192, 18

Kotarba H., Lesch H., Dolag K., Naab T., Johansson P. H., Stasyszyn F. A., 2009, MNRAS, 397, 733

Kraichnan R. H., Nagarajan S., 1967, Physics of Fluids, 10, 859

Kulsrud R. M., Anderson S. W., 1992, ApJ, 396, 606

Kulsrud R. M., Cen R., Ostriker J. P., Ryu D., 1997, ApJ, 480, 481

Mocz P., Pakmor R., Springel V., Vogelsberger M., Marinacci F., Hernquist L., 2016, MNRAS, 463, 477

Monaghan J. J., Lattanzio J. C., 1985, A&A, 149, 135

Morris J. P., 1996, Publ. Astron. Soc. Australia, 13, 97

Mtchedlidze S., Domínguez-Fernández P., Du X., Brandenburg A., Kahniashvili T., O'Sullivan S., Schmidt W., Brüggen M., 2022, ApJ, 929, 127

Müller B., Varma V., 2020, MNRAS, 498, L109

Orszag S. A., Tang C. M., 1979, Journal of Fluid Mechanics, 90, 129

Pakmor R., Springel V., 2013, MNRAS, 432, 176

Pakmor R., Bauer A., Springel V., 2011, MNRAS, 418, 1392

Pakmor R., et al., 2017, MNRAS, 469, 3185

Pakmor R., et al., 2020, MNRAS, 498, 3125

Parker E. N., 1955, ApJ, 122, 293

Parker E. N., 1979, Cosmical magnetic fields. Their origin and their activity. The International Series of Monographs on Physics, Oxford: Clarendon Press

Pattle K., Fissel L., Tahani M., Liu T., Ntormousi E., 2023, in Inutsuka S., Aikawa Y., Muto T., Tomida K., Tamura M., eds, Astronomical Society of the Pacific Conference Series Vol. 534, Protostars and Planets VII. p. 193 (arXiv: 2203.11179), doi:10.48550/arXiv.2203.11179

Phillips G. J., Monaghan J. J., 1985, MNRAS, 216, 883

Powell K. G., Roe P. L., Linde T. J., Gombosi T. I., De Zeeuw D. L., 1999, Journal of Computational Physics, 154, 284

Prada F., Klypin A. A., Cuesta A. J., Betancort-Rijo J. E., Primack J., 2012, MNRAS, 423, 3018

Price D. J., 2012, Journal of Computational Physics, 231, 759

Price D. J., Federrath C., 2010, MNRAS, 406, 1659

Price D. J., Monaghan J. J., 2005, MNRAS, 364, 384

Price D. J., Tricco T. S., Bate M. R., 2012, MNRAS, 423, L45

Price D. J., et al., 2018, Publ. Astron. Soc. Australia, 35, e031 Ruzmaikin A., Sokolov D., Shukurov A., 1988, Nature, 336, 341

Sembolini F., Yepes G., De Petris M., Gottlöber S., Lamagna L., Comis B., 2013, MNRAS, 429, 323

Sembolini F., De Petris M., Yepes G., Foschi E., Lamagna L., Gottlöber S., 2014, MNRAS, 440, 3520

Sembolini F., et al., 2016, MNRAS, 457, 4063

Springel V., 2005, MNRAS, 364, 1105

Springel V., 2010, MNRAS, 401, 791

Springel V., White S. D. M., Tormen G., Kauffmann G., 2001, MNRAS, 328,

Stasyszyn F. A., Elstner D., 2015, Journal of Computational Physics, 282,

Stasyszyn F., Nuza S. E., Dolag K., Beck R., Donnert J., 2010, MNRAS, 408,

Stasyszyn F. A., Dolag K., Beck A. M., 2013, MNRAS, 428, 13

Steenbeck M., Krause F., Rädler K.-H., 1966, Zeitschrift Naturforschung Teil A. 21, 369

Steinwandel U. P., Beck M. C., Arth A., Dolag K., Moster B. P., Nielaba P., 2019, MNRAS, 483, 1008

Steinwandel U. P., Dolag K., Lesch H., Moster B. P., Burkert A., Prieto A., 2020, MNRAS, 494, 4393

Steinwandel U. P., Dolag K., Lesch H., Burkert A., 2022a, ApJ, 924, 26

Steinwandel U. P., Böss L. M., Dolag K., Lesch H., 2022b, ApJ, 933, 131

Steinwandel U. P., Dolag K., Böss L., Marin-Gilabert T., 2023, arXiv e-prints, p. arXiv:2306.04692

Tricco T. S., Price D. J., 2012, Journal of Computational Physics, 231, 7214 Tricco T. S., Price D. J., Bate M. R., 2016a, Journal of Computational Physics, Tricco T. S., Price D. J., Federrath C., 2016b, MNRAS, 461, 1260 Varma V., Müller B., 2021, MNRAS, 504, 636 Vazza F., Dolag K., Ryu D., Brunetti G., Gheller C., Kang H., Pfrommer C., 2011, MNRAS, 418, 960 Vazza F., Brüggen M., Gheller C., Wang P., 2014, MNRAS, 445, 3706 Vazza F., Brunetti G., Brüggen M., Bonafede A., 2018, MNRAS, 474, 1672 Wang P., Abel T., 2009, ApJ, 696, 96 Wissing R., Shen S., 2023, A&A, 673, A47 Wurster J., Price D., Ayliffe B., 2014, MNRAS, 444, 1104 Wurster J., Price D. J., Bate M. R., 2016, MNRAS, 457, 1037 Wurster J., Price D. J., Bate M. R., 2017, MNRAS, 466, 1788 Wurster J., Bate M. R., Price D. J., 2018, MNRAS, 475, 1859 Wurster J., Bate M. R., Price D. J., 2019, MNRAS, 489, 1719 Xu S., Lazarian A., 2020, ApJ, 899, 115 Zel'dovich Y. B., 1970, Soviet Ast., 13, 608

van de Voort F., Bieri R., Pakmor R., Gómez F. A., Grand R. J. J., Marinacci

APPENDIX A: IDEALISED TESTS

A1 Divergence Advection Test

F., 2021, MNRAS, 501, 4888

We start with the popular divergence advection test as it has been carried out by several groups to test divergence cleaning schemes in SPH. The test is initialized in a periodic domain with 0.0 < x < 2.0, 0.0 < y < 2.0, and 0.0 < z < 0.1 we note that we carry the test out in three spatial dimensions where the z-direction is factor of 20 thinner than the x and y directions. The test is carried out with a Wendland C4 kernel where we do not apply the nonphysical kernel bias correction of Dehnen & Aly (2012). The density is initialized as $\rho = 1$, the pressure as P = 6 and we adopt $\gamma = 5/3$ with an equation of state as $P = \rho u(\gamma - 1)$. The divergence perturbation is advected with $v_x = v_y = 1$. We set v_z to zero. The magnetic field is set to $B_x = B_y = 0$, except for a small perturbation within the x-component of the magnetic field given via:

$$B_{\rm x} = \frac{1}{4\pi} \left[\left(\frac{r}{r_0} \right)^8 - 2 \left(\frac{r}{r_0} \right)^4 + 1 \right],\tag{A1}$$

with $r = \sqrt{x^2 + y^2}$ and $r_0 = 1/\sqrt{8}$. The z-component of the magnetic field is set to $B_z = 1/\sqrt{4\pi}$. The conditions lead to a β around 150. Since the β is high there is not necessarily the need to correct for Tensile-instability hence we switch it off, alongside the artificial resistivity to test energy conservation of the method. These are the same settings as adopted by Tricco et al. (2016a). The particle positions are initialized on a hydrodynamical glass distribution with 512,000 particles, which is obtained by running the code with very large viscosity until equilibrium is reached. This is again different from the procedure in Tricco et al. (2016a), who simply adopted particles based on a triangular lattice. In Fig. A1 we show the results of the test simulation to validate the basic functionality of the the method in the simulation code Gadget. The top row shows the results with no cleaning applied, the second row shows the results without parabolic (only hyperbolic) cleaning terms, and the third row shows the full scheme that implements both, the hyperbolic and parabolic cleaning terms with available cleaning speed. In the bottom row, we demonstrate a simulation in which the cleaning speed is 2 times faster than the fastest wave speed in the simulation, to demonstrate that our implemented timestep limiter for the cleaning speed is working properly. In Fig. A2 we show the time evolution of the divergence of the magnetic field for our 4 advection tests. This test clearly demonstrates that the divergence error is preserved when no cleaning is applied. In the case in which we only allow for hyperbolic cleaning, the situation becomes worse because there is no damping of the waves introduced by the hyperbolic term alone. However, the divergence error is reduced by about an order of magnitude when the fiducial scheme in row three is applied.

A2 Orszag-Tang Vortex

The next test we perform is the Orszag-Tang-Vortex test Orszag & Tang (1979). Hereby, we closely follow the setup of Tricco et al. (2016a). Particle positions are again initialized via a hydrodynamical glass distribution with 512,000, with density $\rho=25/36|pi$, pressure $P=5/12\pi$, velocity $v_x=-\sin 2\pi \cdot y$, $v_y=\sin 2\pi \cdot x$, $v_z=0$, and magnetic field $B_x=-\sin 4\pi \cdot y$, $B_y=-\sin 2\pi \cdot x$ and $B_z=0$, in 3D periodic domain, which spans 0.0 < x < 1.0, 0.0 < y < 1.0, and 0.0 < z < 0.1. We show the result of the test for simulations without cleaning (top row), with hyperbolic cleaning only (center row), and with the constrained divergence cleaning (bottom row), for four different points in time at t=0.25, t=0.5, t=0.75, and t=1.0 in Fig. A3. We show the time evolution of the divergence error for these simulations in Fig. A4.

A3 Brio-Wu Shocktube

Finally, we tested the scheme against a Brio-Wu shock tube Brio & Wu (1988). The test is realized within a three-dimensional domain with extent 0.0 < x < 140, 0.0 < y < 1, and 0.0 < z < 1 with periodic boundary conditions. The test itself is realized with a total of 600,000 particles on a glass-like distribution. The shock tube has an initial left-hand state given via $[\rho, P, v_x, v_y, v_z, B_x, B_y, B_z] = [1, 1, 0, 0, 0, 0, 0.75, 1, 0]$ and an initial right hand state given via $[\rho, P, v_x, v_y, v_z, B_x, B_y, B_z] = [0.125, 0.1, 0, 0, 0, 0.75, -1, 0]$. We performed three versions of this test case, without cleaning (Fig. A5), with hyperbolic cleaning only , and with the fiducial scheme that is realizing the combination of hyperbolic and parabolic cleaning (Fig. A6).

APPENDIX B: COSMOLOGICAL TESTS

One addition in this work compared to previous implementations of the constrained cleaning scheme (e.g. Tricco et al. 2016a; Wissing & Shen 2023) is its application to cosmological simulations. We will use two popular cosmological test cases to validate that the scheme is working in co-moving units as intended.

B1 Magnetized Zeldovich Pancake

The Zeldovich-pancake is a validation test to demonstrate the basic capabilities of a code to integrate a system in a co-moving unit system. The goal of this test is less to show that the cleaning scheme is working but rather to show that it is not interfering with the expected analytic solution of the unmagnetized problem. The test has been introduced by Zel'dovich (1970) and is well suited to test high Mach number flows in combination with highly anisotropic particle distributions and low specific internal energies. The test is initialized at a redshift of $z_i = 100$ with a single sine wave perturbation in the density field which will be tracked down to redshift $z_c = 1$ at which it

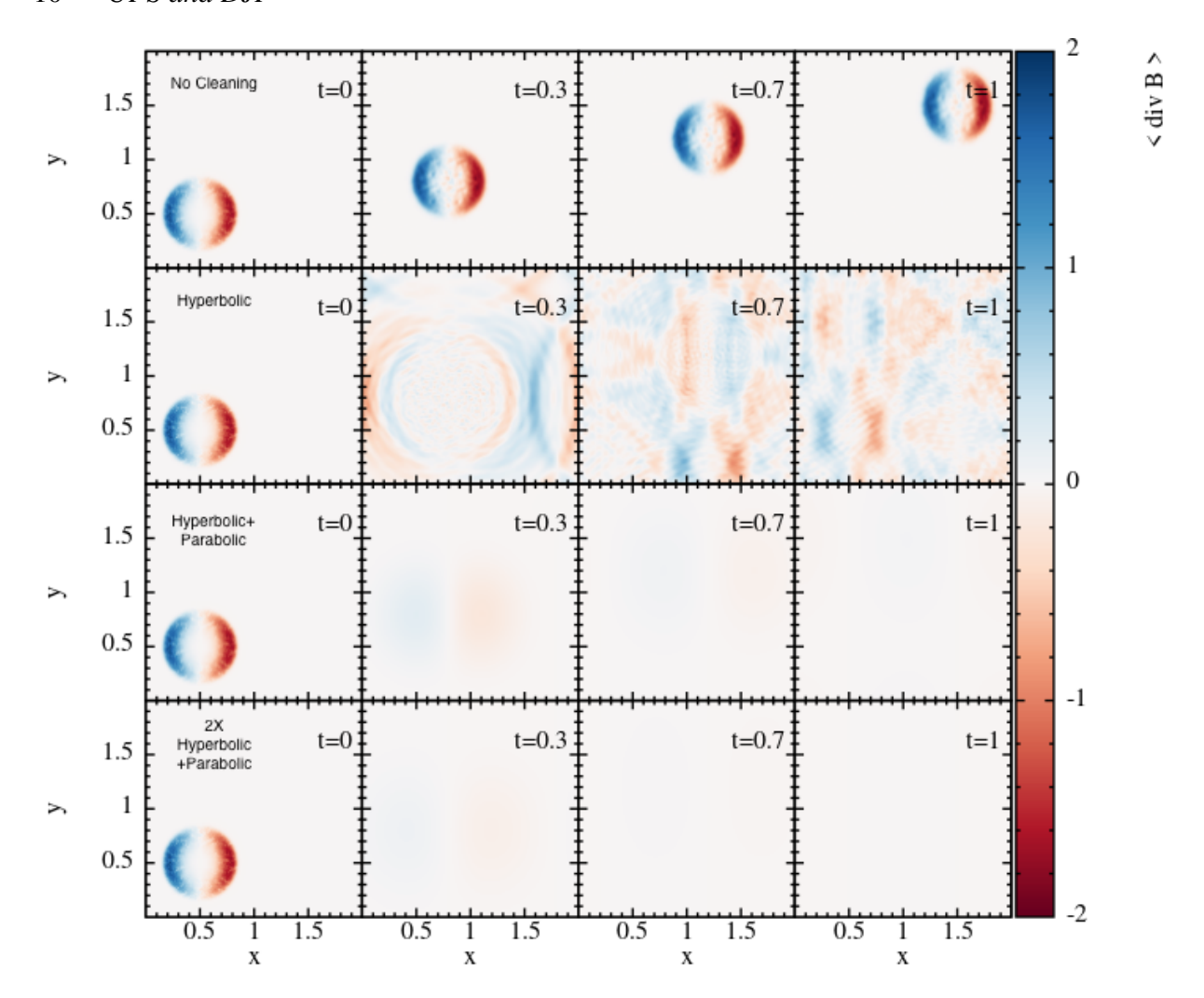


Figure A1. Divergence advection test of an artificially introduced divergence error in the systems that is advected alongside the diagonal. We present four simulation runs with no cleaning (top row), hyperbolic cleaning only (second row), hyperbolic and parabolic cleaning (third row, fiducial model) as well as a fourth run with parabolic and hyperbolic cleaning that allows for a faster cleaning speed than the fastest wave speed by a factor of two.

is transitioning to the caustic formation that we follow all the way down to redshift zero. The initial conditions are as follows:

$$x = x_{i} - \frac{1 + z_{c}}{1 + z} \frac{\sin(kx_{i})}{k},$$
(B1)

$$\rho = \frac{\rho_0}{1 - \frac{1 + z_c}{1 + z} \cos(kx_i)},\tag{B2}$$

$$v_{\text{pec}} = -H_0 \frac{1 + z_{\text{c}}}{\sqrt{1 + z} \frac{\sin(kx_i)}{k}} \hat{\mathbf{x}},$$
(B3)

$$T = T_{\rm i} \left(\frac{1 + z_{\rm c}}{1 + z} \right)^2 \left(\frac{\rho(x, z)}{\rho_0} \right)^{2/3},\tag{B4}$$

with the unperturbed position x, the critical density of the Universe ρ_0 , the Hubble constant $H_0=100~\rm km~s^{-1}~Mpc^{-1}$, $z_c=1$ and initial temperature $T_i=100\rm K$. The test is realized at the very low resolution of 32^3 particles. Additionally, we adopt an initial seed field in the y-direction of 10^{-3} physical G at redshift $100~(9.80\times10^{-7}$ co-moving G). The test itself is unspectacular as the field is simply following the density perturbation. We show the results of the test

in Fig. B1. We note that the cleaning scheme has almost zero effect in this particular test. We show the peculiar (x component) of the velocity field on the left, the magnetic field in the center panel, and the divergence error on the right for runs without cleaning (top row), with the fiducial cleaning (center row) and the fiducial cleaning where we adopt a cleaning speed that is a factor of two faster than the fastest wave speed. In the latter case, we see some minor reduction in the divergence error, but the effect is minor compared to the fiducial cleaning and no cleaning cases. However, the test is useful to test if the conversion of the cleaning scheme to co–moving units has been carried out correctly, which appears to be the case.

This paper has been typeset from a $T_EX/I = T_EX$ file prepared by the author.

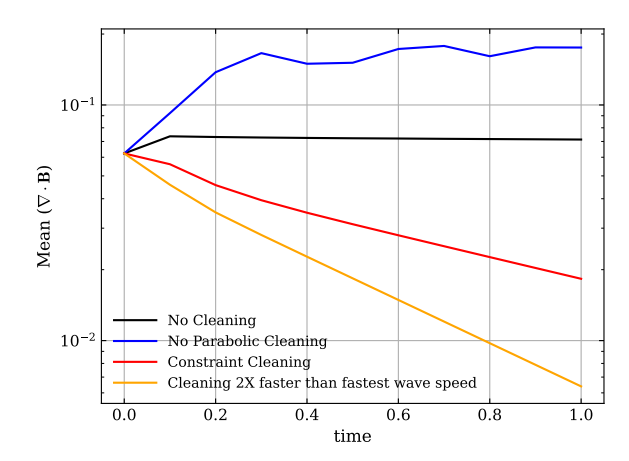


Figure A2. We show the time evolution of the mean value of the divergence of the magnetic field for the four advection tests carried out. In the absence of cleaning, we find that the code is preserving the initial divergence error (black line). For hyperbolic cleaning only we find that the code is increasing the mean value of the divergence compared to the reference run without cleaning but stabilizes at a higher value by around a factor of 2. For the fiducial cleaning scheme, we find that the divergence error is reduced by the end of the simulation by around a factor of 5 (red line). If we allow for cleaning speeds that are 2 times faster than the fastest wave speed we find an improvement by a factor of 10 at t=1.

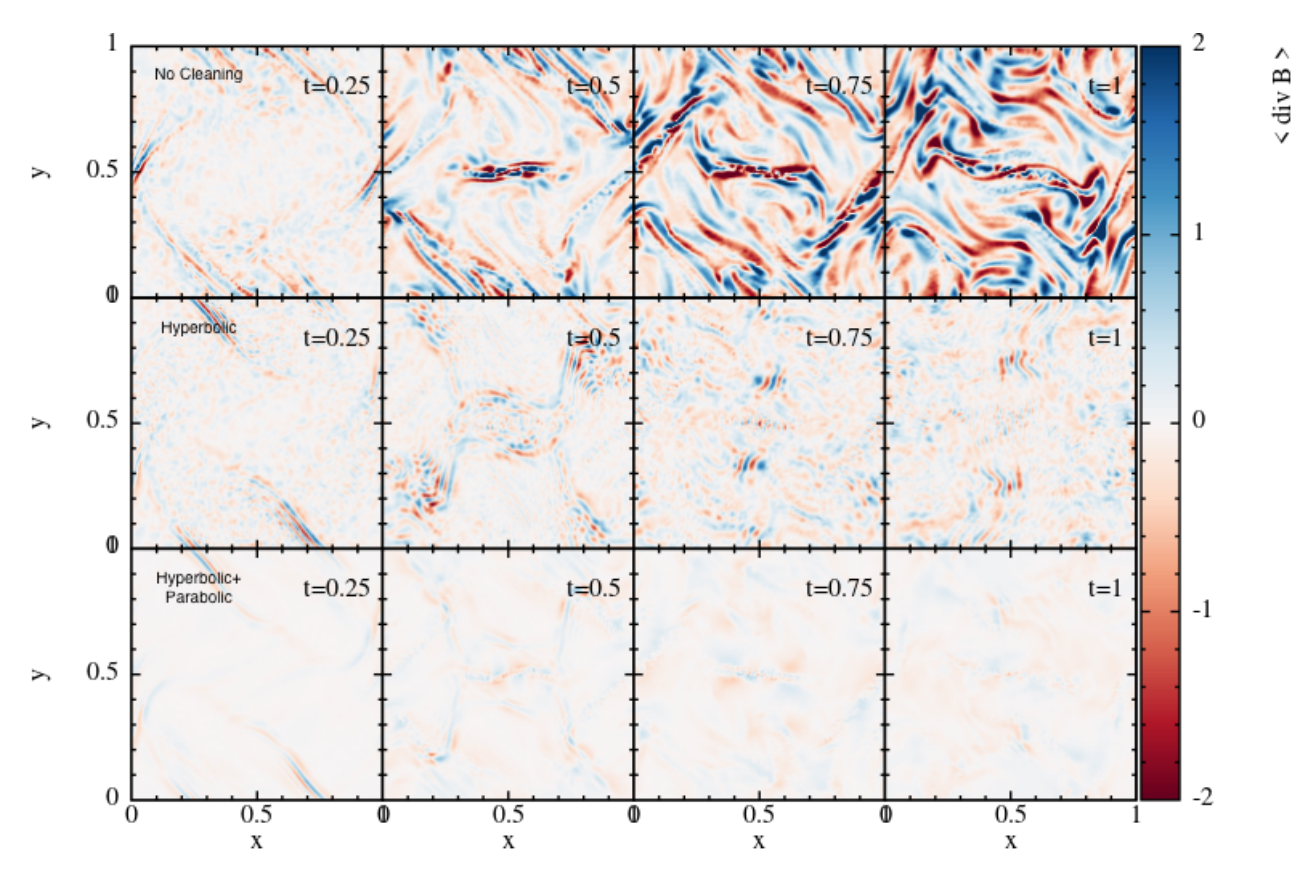


Figure A3. Divergence advection test of the Orszag-Tang vortex' divergence error. We present four simulation runs with no cleaning (top row), hyperbolic cleaning only (second row), hyperbolic and parabolic cleaning (third row, fiducial model) as well as a fourth run with parabolic and hyperbolic cleaning that allows for a faster cleaning speed than the fastest wave speed by a factor of two.

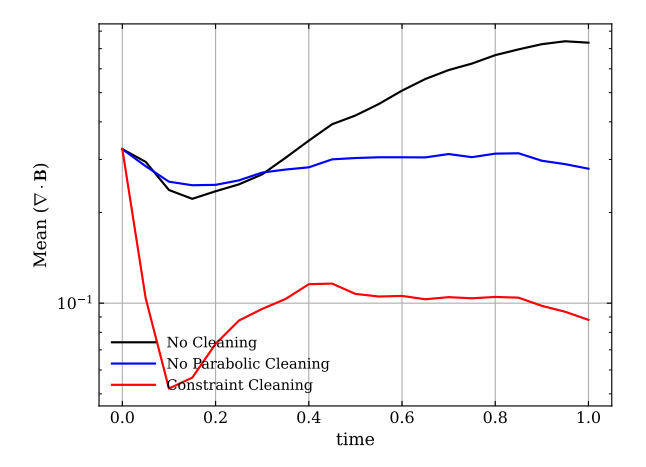


Figure A4. We show the time evolution of the mean value of the divergence of the magnetic field for the four advection tests carried out. In the absence of cleaning, we find that the code is preserving the initial divergence error (black line). For hyperbolic cleaning only we find that the code is increasing the mean value of the divergence compared to the reference run without cleaning but stabilizes at a higher value by around a factor of 2. For the fiducial cleaning scheme, we find that the divergence error is reduced by the end of the simulation by around a factor of 5 (red line). If we allow for cleaning speeds that are 2 times faster than the fastest wave speed we find an improvement by a factor of 10 at t=1.

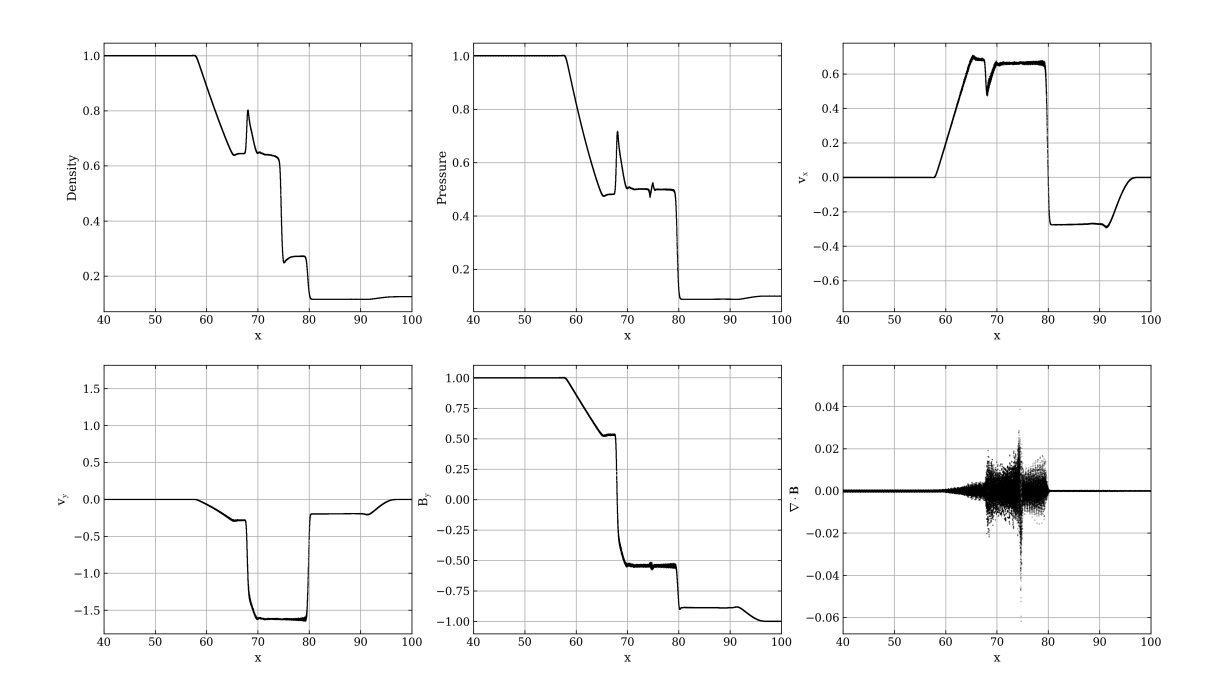


Figure A5. Simulation of a Brio-Wu shock tube at t=7. We show the density (top left), the pressure (top center), the x-velocity (top right), the y-velocity (bottom left), the y-component of the magnetic field (bottom center), and the divergence of the magnetic field (bottom right).

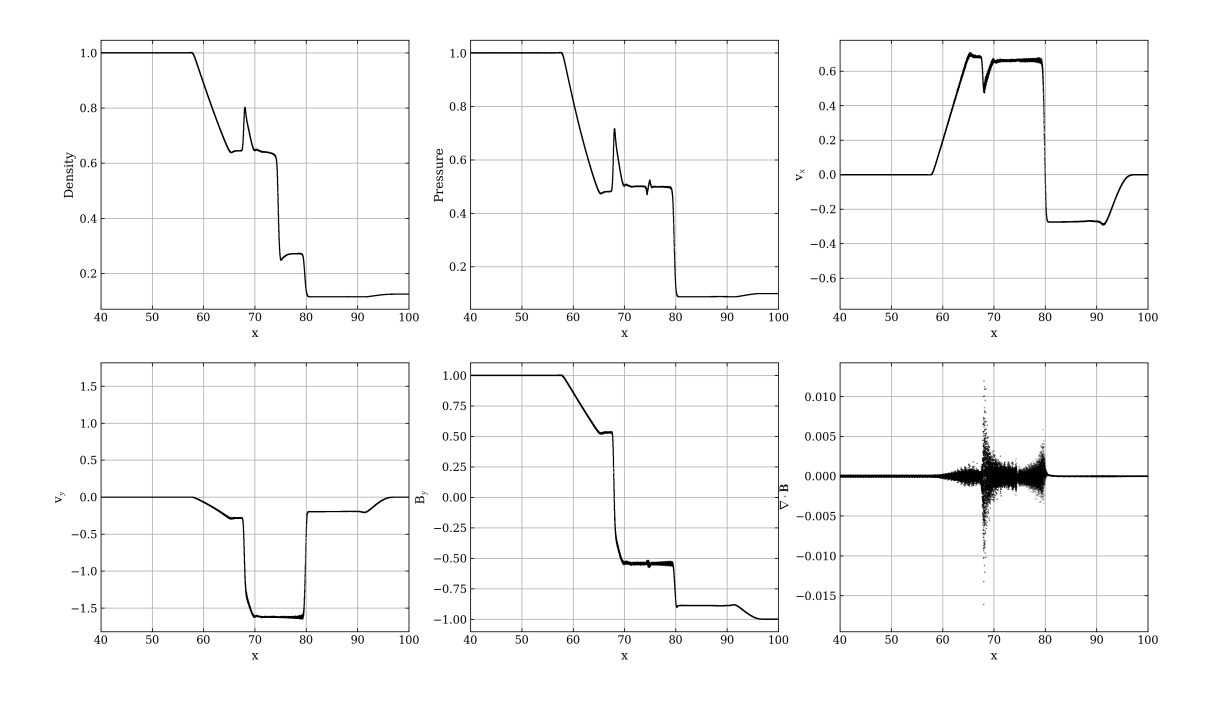


Figure A6. Same as Fig. A5 but for a simulation includes the hyperbolic and parabolic cleaning terms (fiducial model).

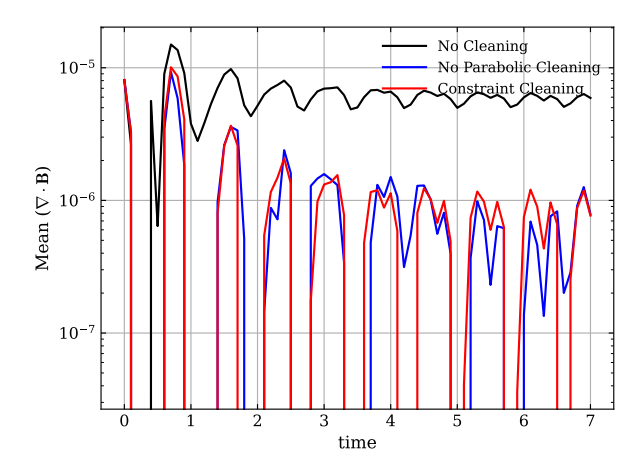


Figure A7. We show the time evolution of the mean value of the divergence of the magnetic field for the four advection tests carried out. In the absence of cleaning, we find that the code is preserving the initial divergence error (black line). For hyperbolic cleaning only we find that the code is increasing the mean value of the divergence compared to the reference run without cleaning but stabilizes at a higher value by around a factor of 2. For the fiducial cleaning scheme, we find that the divergence error is reduced by the end of the simulation by around a factor of 5 (red line). If we allow for cleaning speeds that are 2 times faster than the fastest wave speed we find an improvement by a factor of 10 at t=1.

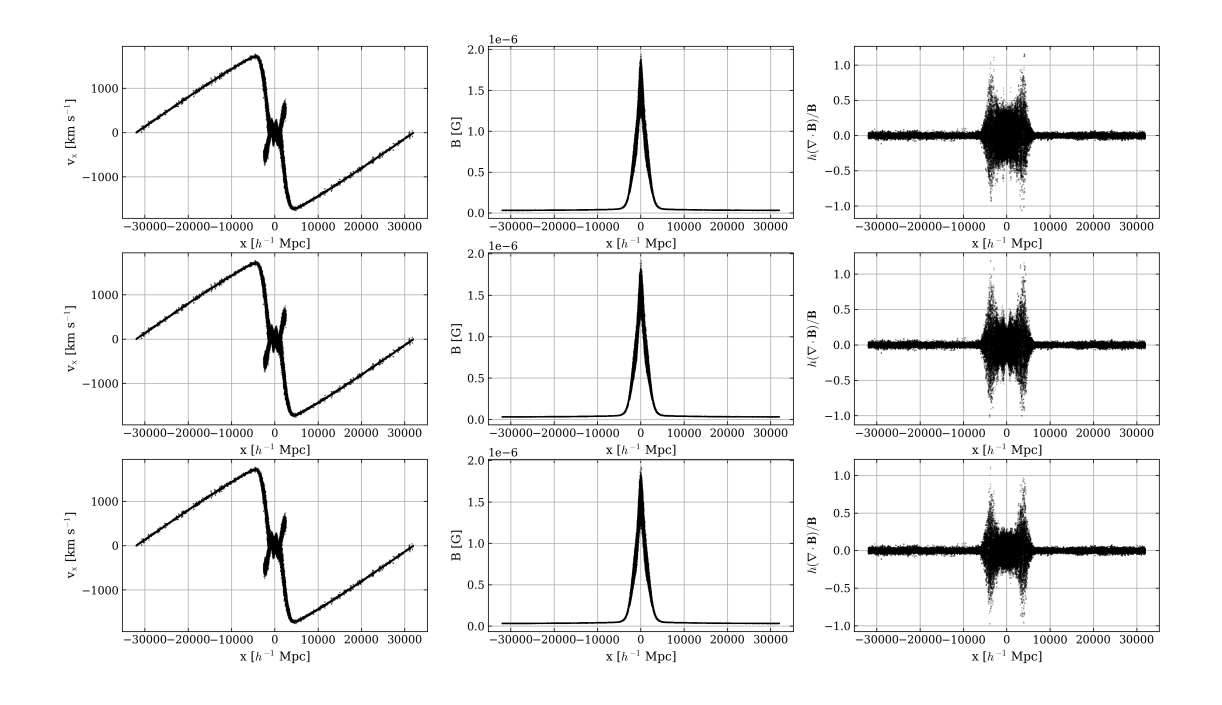


Figure B1. Results of the magnetized Zeldovich pancake test